Dynamics of neutrals and ions in an ultrafast laser produced Zn plasma

N. Smijesh, Kavya H. Rao, and Reji Philip[a)]
Ultrafast and Nonlinear Optics Lab, Light and Matter Physics Group, Raman Research Institute, Bangalore 560080, India

(Received 13 February 2015; accepted 2 March 2015; published online 13 March 2015)

Optical time of flight dynamics of neutrals and ions in an ultrafast laser produced zinc plasma generated by irradiating a solid zinc target using 100 fs laser pulses is investigated. An acceleration of ions is observed which arises from internal Coulomb forces acting between charged species in the plasma. Some of the fast ions recombine with electrons in the plasma and generate fast neutrals. Plasma plume imaging performed at various ambient pressures indicates adiabatic expansion at lower pressures and plume front deceleration at higher pressures: at lower pressures the plume front-time (R-t) plot displays a linear expansion, shock wave model fits to the data at 5 Torr and at higher pressures the data fits better to the drag model. Furthermore, around an intermediate pressure of 10 Torr, the R-t plot fits to the shock wave model at earlier stages of plasma expansion, while it fits to the drag model at the later stages. These investigations provide relevant information on the acceleration of ions and neutrals in an expanding zinc plasma plume produced by ultrafast laser pulses. © *2015 AIP Publishing LLC*.
[http://dx.doi.org/10.1063/1.4914928]

I. INTRODUCTION

Laser produced plasma (LPP) is transient in nature and the properties change instantaneously with space and time, causing rapid expansion and dynamic changes in the generated plume. Investigation of plasma expansion dynamics and kinetics in the presence of an ambient gas is important for optimizing various applications of ultrafast laser ablation such as pulsed laser deposition (PLD),[1] nanoparticle generation,[2] higher harmonic generation (HHG),[3] and EUV production.[4] In pulsed laser ablation, the energy absorbed by electrons in the system is coupled to the lattice via phonon(s), and the time scales of energy deposition are determined by the laser pulse duration.[5] Excitation laser pulse width is of particular relevance in understanding the fundamental physical processes that occur at short time scales, such as excitation, melting, and material ablation. These are temporally separated in the case of ultrafast ablation using femtosecond (fs) laser pulses.[6] In a fs ablation process, excitation happens in fs time scales, followed by material ablation in 1–10 ps.[7,8] Two promising methods for describing the ablation process using fs pulses are the plasma-annealing model[9] and two-temperature model.[10] Ablation of materials using fs irradiation results in the formation of fast ions, fast and slow neutrals, nanoparticles, and nanoclusters, which occur at different time scales.[11,12]

In this work, experimental investigation of the time of flight dynamics of neutrals and ions in an LPP generated in a solid zinc target by ultrafast laser pulses (100 fs, 800 nm), at an irradiation fluence of 10 J/cm^2, is carried out. Nitrogen is used as the ambient gas. Velocities of ions and neutrals measured at various axial points in the plasma plume reveal an acceleration of both species at distances close to the target surface, before being decelerated via plume-background interaction. ICCD imaging of the plasma plume at appropriate time scales shows evidence of plume front deceleration, even while the species inside may be accelerating. Motion of the plume front is plotted as a function of time, which is fitted to standard models such as adiabatic expansion, shock wave model, and drag model,[13–15] for different ambient pressures and time scales.

II. EXPERIMENT

A regeneratively amplified Ti: Sapphire laser (*TSA-10, Positive Light*) delivering 100 fs, 10 mJ pulses at 800 nm was used for target excitation. Laser pulse energy is attenuated to 4 mJ using a half wave plate and cube beam polarizer, and the beam is focused using a 50 cm plano-convex lens to ~100 μm spot size on the surface of a 99.99% pure zinc target (*ACI Alloys Inc, USA*) kept in a nitrogen background, to generate the plasma. Visible light emitted from the plasma at various pressures is recorded using a monochromator (*iHR 320, Jobin Yvon Horiba*) equipped with a CCD (*Synergy, Jobin Yvon Horiba*), and the spectral lines obtained are identified by comparing them with the standard NIST database.[16] Optical Time of Flight (OTOF) measurements of neutrals and ions are performed at 481 nm [4S 5S $^3S_1 \rightarrow$ 4S 4P $^3P_2$] and 491 nm [4f $^2F_{5/2} \rightarrow$ 4d $^2D_{3/2}$], respectively, under nitrogen pressures of 5 Torr, 10 Torr, 50 Torr, and 100 Torr. OTOF spectra are recorded using a fast photomultiplier tube (PMT—*R943-02*, *Hamamatsu,* rise time ~ 3 ns) attached to one of the exit slits of the monochromator. PMT signals are recorded, digitized, and stored using a fast oscilloscope (*DPO 7354, Tektronix*) for further analysis. To understand the expansion dynamics of the plume, the LPP is imaged at various times for various pressures using an Intensified Charge Coupled Device (ICCD—*4 Picos, Stanford Computer Optics Inc*., *USA*), which is positioned

a)Author to whom correspondence should be addressed. Electronic mail: reji@rri.res.in

perpendicular to the direction of plasma expansion. Imaging is done by an f/2.8 aperture lens (*Nikon, Micro-NIKKOR—5* mm) attached to the ICCD. Details of OTOF measurements and ICCD imaging of the fs laser produced zinc plasma are presented in Secs. III A–III C.

III. RESULTS AND DISCUSSION

Minimal heat diffusion and absence of plasma shielding are the major features of fs laser produced plasmas. Ejection of particles happens from the target surface well after the arrival of the laser pulse, allowing efficient coupling of the laser energy to the target surface.[5] Material ablation happens if the intensity of irradiation exceeds the ablation threshold, which is given by[17]

$$F_{th} = \frac{3}{8}(\varepsilon_b + \varepsilon_{esc})\frac{\lambda n_e}{2\pi} \quad (1)$$

for short laser pulses, where ε_{esc} is the work function (4.33 eV/atom), λ is the wavelength of irradiation (8×10^{-5} cm), and n_e is the number density of conduction electrons (6×10^{22} cm^{-3}). Substituting these values to Eq. (1) gives $F_{th} = 0.265$ J/cm^2. With a laser fluence ~ 10 J/cm^2 which is well above the ablation threshold, material ablation occurs within picoseconds and plasma is formed. Coulomb explosion, phase explosion, fragmentation, and thermal vaporization are the major mechanisms responsible for ablation.[18]

Optical Emission Spectroscopic (OES)[19] characterization of the generated zinc plasma was performed for various background pressures to understand the emission characteristics and to determine the pressure at which maximum emission occurs. Measured spectra include emissions from neutrals at 334.5 nm, 468 nm, 472 nm, and 481 nm, which are intense when compared to the emission intensity of ions at 491 nm and 492 nm, as seen from Figure 1. This result is in agreement with the observation that fs LPPs are neutral rich.[20,21] At larger irradiation intensities, thermal vaporization is known to be responsible for the generation of neutrals within the plume, as most of the ablated species will reach the vaporization temperature of the target material. Emission intensity measured at 50 Torr for 481 nm are ~9 to 10 times larger than that observed at lower pressures (i.e., from 1×10^{-6} Torr to 5×10^{-1} Torr) and ~1.5 times larger than that observed at higher pressures, i.e., at 5 Torr, 150 Torr, and 200 Torr. These measurements show that emission intensity maximizes within an optimum range of pressures (5 Torr–100 Torr in the present case) where it may be assumed that thermal leak to the surroundings is minimal and collisions among the plasma species is maximal.[22] This observation is in support of existing experimental results reported by Farid *et al.*[23] and Smijesh *et al.*[24] We also performed OTOF studies for 10 Torr, 50 Torr, and 100 Torr background pressures, for various axial positions in the expansion direction of the plume. The effects of pressure and position on the OTOF of neutrals at 481 nm and ions at 491 nm are presented in Secs. III A and III B.

A. Effect of ambient pressure

The temperature and number density of LPP plumes are found to increase with pressure and reach a maximum value in the range of milli Torr to tens of Torr pressures, beyond which they are found to decrease.[25] At lower pressures the plume expands adiabatically, and collisions are minimal, reducing the number density. On the other hand at higher pressures, effects such as plume confinement, plume sharpening, and plume splitting will alter the plume structure substantially.[26] The plume loses more energy via collisions with increase in background pressure because cooling, which is

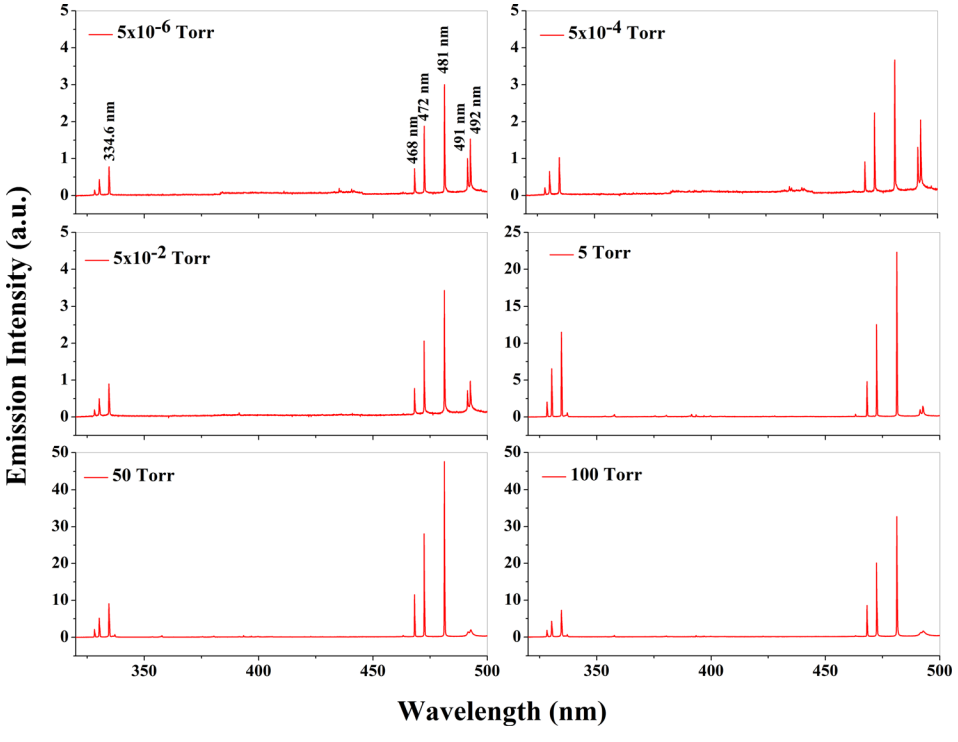

FIG. 1. Emission spectra of the femtosecond laser produced zinc plasma plume measured for the background pressures of 5×10^{-6} Torr, 5×10^{-4} Torr, 5×10^{-2} Torr, 5 Torr, 50 Torr, and 100 Torr. Emission intensity is found to maximize at 50 Torr in the present case. Measurements are done at a distance of 1 mm from the target surface.

given by $Q_{\Delta t} = \frac{2m_e}{M_B}\sigma_{ea} n_B \left[\frac{5kT_e}{\pi m_e}\right]^{1/2}$, is directly proportional to the density of the background gas.[27] Here, n_B and M_B are the density and mass of the background gas, respectively, σ_{ea} is the elastic scattering cross section of the electrons, and kT_e is the plasma thermal energy. It is clear from published results[25] that within a certain range of optimum pressures number density is high due to species interactions within the plume and plume—background interaction.

Figure 2 depicts OTOF measurements performed at 10 Torr for neutrals (Zn I) and ions (Zn II) at various axial positions in the expanding plasma plume. Emission could be detected up to 6 mm and 4 mm distances for Zn I and Zn II, respectively. At 1 mm distance emission from Zn II is found to be stronger compared to that from Zn I at the inner region of the plasma. Emission is found to have a relatively longer history for neutrals and shorter history for ions. OTOF measured at 50 Torr (see Figure 3) displays emission intensities similar to those measured at 10 Torr for Zn II, whereas the intensities are higher for Zn I. Plasma confinement limits emission from both species to smaller distances, which in turn results in emission being detected only up to 4.5 mm for Zn I and 3 mm for Zn II. OTOF measurements at 100 Torr (see Figure 4) show reduced emission intensities for both Zn II and Zn I compared to those measured at similar positions for 10 Torr and 50 Torr. At high pressures plasma confinement and thermal leak to the surroundings limit the emission from both species to smaller distances. Emission could be detected up to 3 mm for Zn I and 2.5 mm for Zn II at 100 Torr.

There are previous reports on the generation of fast and slow neutrals at different timescales in an expanding laser produced plasma depending on the irradiation conditions.[12,22,24] For example, fast neutrals arrive within 100 ns to 200 ns, whereas slow neutrals arrive around 300 ns to 500 ns or more, at close distances to the target.[28] Moreover, it has been experimentally found that fast neutrals display a fast rise in the OTOF spectra compared to slow neutrals.

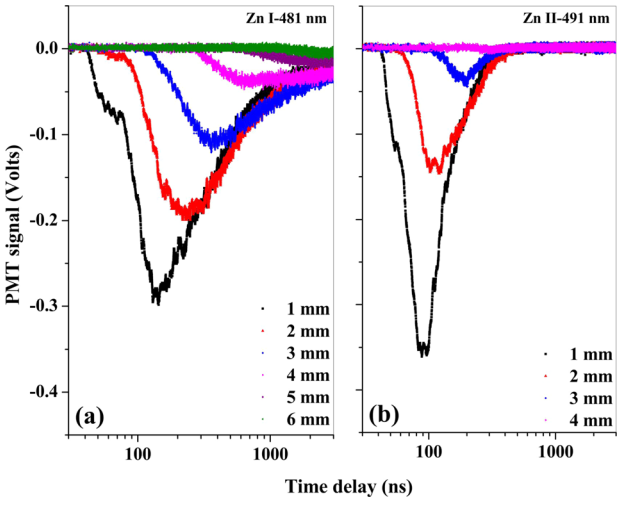

FIG. 2. Optical time of flight measurements of (a) neutrals (Zn I) at 481 nm and (b) ions (Zn II) at 491 nm for various positions in the plasma plume, measured at the background pressure of 10 Torr. It is found that emission from ions is stronger compared to that of neutrals in the inner region of the plume.

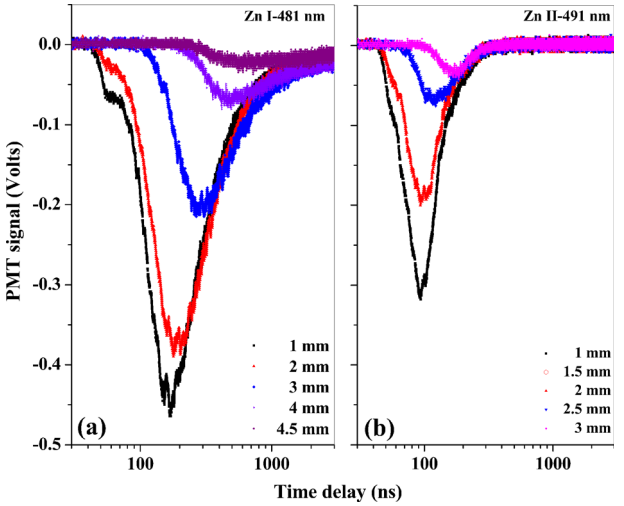

FIG. 3. Optical time of flight measurements of (a) neutrals (Zn I) at 481 nm and (b) ions (Zn II) at 491 nm for various positions in the plasma plume, measured at the background pressure of 50 Torr. Emission from neutrals is stronger compared to that from ions due to large recombination.

From the present OTOF profiles (see Figures 2–4), it is found that neutrals display a fast rise followed by a slow decay. These profiles may be the convolution of fast (recombined) and slow (un-ionized) neutrals arriving at different times which are not well resolved in time. Fast ionic species recombine with slow electrons (through a three body recombination process) to generate excited neutrals, which is one of the reasons for the presence of neutrals up to a larger distance in the plume. The persistence of emission (which was measured by taking the $1/e^2$ intensity values of the OTOF signals) is found to be higher for neutrals compared to that for ions. For neutrals the emission lasts up to 3.5 μs, 1.8 μs, and 1.5 μs, while for ions it lasts only up to 450 ns, 350 ns and 300 ns, for ambient pressures of 100 Torr, 50 Torr, and 10 Torr, respectively. Moreover, OTOF signals from neutrals are found to maximize at 50 Torr in the present case, confirming the results of optical emission spectroscopic studies where the emission was found to maximize at ~50 Torr.

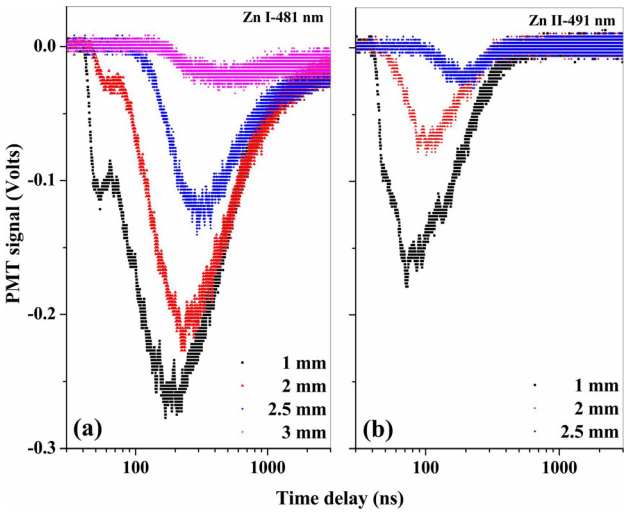

FIG. 4. Optical time of flight measurements of (a) neutrals (Zn I) at 481 nm and (b) ions (Zn II) at 491 nm for various positions in the plasma plume, measured at the background pressure of 100 Torr.

B. Velocity of neutrals and ions

Velocities of the neutral and ionic species can be calculated by knowing the position of measurement and time of arrival of corresponding peaks in the recorded OTOF traces. Calculated velocities plotted against axial positions are shown in Figure 5 for different pressures, where the error bar is estimated from multiple measurements. It is found that the velocity of ions increases up to a certain distance and then decreases, irrespective of the ambient pressure. For example, at 50 Torr pressure the velocity of neutrals doubles from ~5.5 km/s to ~11 km/s within a distance of 2 mm (travelling from 1 mm to 3 mm) whereas the velocity of ions increases from ~11 km/s to ~22 km/s within a distance of 1.5 mm (travelling from 1 mm to 2.5 mm), indicating an acceleration for both species. Both neutrals and ions follow a similar trend in the variation of velocity with respect to axial position in the plasma plume, even though neutrals are found to move with a velocity lesser than that of ions. The initial velocity increase and subsequent decrease can be explained as follows: acceleration of ions occurs due to space-charge effects,[29–31] i.e., the pull of the bunch of electrons moving ahead due to its larger thermal energy in the plume, and push of other ions present near the emitters (e.g., near Zn II). Emitter-perturber interactions[32–34] which are stronger in the case of ions by virtue of their charge cause them to move with a larger velocity as shown in Figure 5.

Velocities of the generated electrons, ions, and neutrals in the LPP vary as a function of their thermal energies. The high temperature of plasma soon after ablation leads to thermal expansion of the plume[35] creating an electric field inside the plume. This electric field interacts with the charged particles, causing them to accelerate along the expansion direction depending on the intensity of the generated electric field. It is reported that space-charge effects present in the LPP plume can accelerate ions to a certain distance.[29–31]

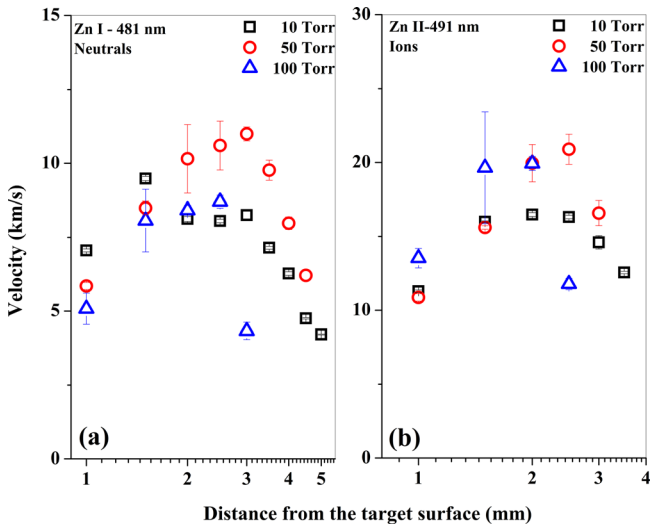

FIG. 5. Velocities of peaks corresponding to (a) neutrals and (b) ions in the plume, plotted against the distance of measurement from the target surface. Error bars are calculated from multiple measurements. Ions are found to accelerate near the target surface. Since some of the accelerating fast ions recombine with the slow electrons in the plume to generate fast neutrals, an acceleration of neutrals also can be observed.

When accelerating fast ions recombine with slow electrons in the plume, fast neutrals are generated. The generated fast neutrals gain energy through collisions and transfer of thermal energy to kinetic energy, causing them to accelerate to short distances close to the target. Emission from neutrals has a longer history spanning microseconds, due to the presence of recombined as well as un-ionized neutrals in the plasma.

C. Plume imaging

Interaction of LPP with the ambient gas leads to plasma plume expansion involving several physical processes such as thermalization, attenuation, diffusion, electron-ion recombination, and shock wave formation, which is rather a complex phenomenon.[5] Since the nature and pressure[26] of the ambient gas influences the hydrodynamics of the plume, we performed fast imaging of the plasma using an ICCD for a range of ambient pressures (0.05 Torr–100 Torr). All images are spectrally integrated from 300 nm to 900 nm, which constitutes emission from various species such as excited neutrals and ions. The plasma plume expands freely at low pressures exhibiting free adiabatic expansion, and the interaction between plasma and surrounding gas is negligible. On the other hand, at higher ambient pressures plume dynamics is characterized by a stronger interpenetration of the background gas with the plume. At still higher pressures, expansion dynamics of the plasma is fully determined by the properties and nature of the ambient gas. Shock wave formation and slowing of the plume due to spatial confinement of the plasma happen at higher pressures.[36,37]

For sufficiently high pressures, when the ablated mass is small compared to the mass of the background gas in motion, a shock wave front is created. During the earlier stages of plasma expansion, its propagation can be explained using the shock wave model by a simplified Taylor-Sedov solution to the point blast problem for spherically expanding plasmas,[38,39] which is given by

$$z = \left(\frac{E_0}{\rho_b}\right)^{\frac{1}{5}} t^{\frac{2}{5}} + z_0, \tag{2}$$

where z is the distance from the target, E_0 is a constant proportional to the laser energy density, ρ_b is the density of the background gas, and z_0 is the distance moved by the species during a time of the order of the average life time of the excited states. At lower ambient pressures when the mass of the ejected species is higher than that of the background gas in motion, the ejected species will slow down obeying a classical drag force model[40] which can be expressed as

$$z = z_f[1 - \exp(-\beta t)] + z_0, \tag{3}$$

where β is the slowing coefficient, and z_f $(= \frac{v_0}{\beta})$ is the stopping distance of the plume where v_0 is the initial velocity of the ejected species.

We carried out plume imaging for various gate delays (GD) with a fixed gate width (GW) of 5 ns. Though the relatively small 5 ns GW would reduce image intensity, it was chosen to ensure that even small fluctuations in the plasma

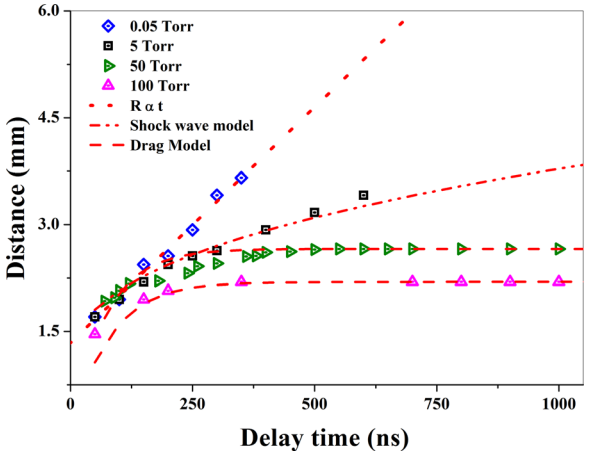

FIG. 6. Plume front–time (R-t) plots for low and high ambient nitrogen pressures, calculated from the ICCD images. Symbols represent data and dashed lines represent plume expansion models. Free expansion model fits at 0.05 Torr, shock wave model fits at 5 Torr, and drag model fits at 50 Torr and 100 Torr. A small deviation from the drag model seen at 50 Torr for ≤400 ns may be due to shock wave effects present in the earlier stages of expansion.

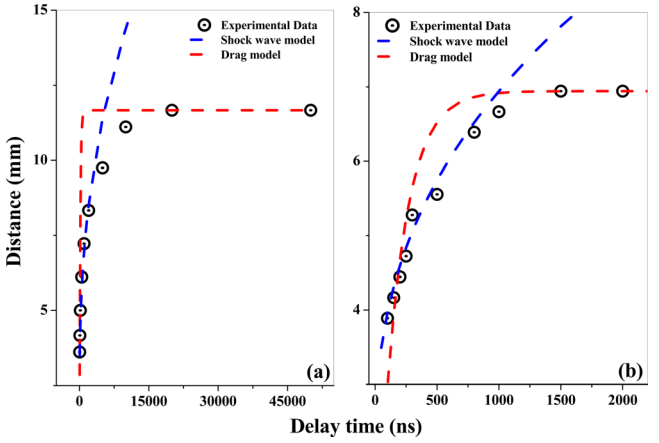

FIG. 8. Plume front-time (R-t) plots for an intermediate ambient pressure of 10 Torr, calculated from the ICCD images. Symbols represent data while blue dashed lines give the shock wave model and red dashed lines give the drag model. Data fits better to the shock wave model at earlier stages and to the drag model at later stages, of expansion. (a) 10% of gate delay as gate width, (b) 10 ns as gate width.

could be captured. From the ICCD images, the position of the plume front can be measured for various gate delays, and a graph displaying position versus time (R-t) can be plotted, as shown in Figure 6. It is found that at the ambient pressure of 0.05 Torr the plume front shows adiabatic expansion allowing a linear fit to the R-t plot. At 5 Torr the shock wave model fits to the R-t plot in the initial stages, and then the plume front is found to decelerate. At still higher pressures (50 Torr and 100 Torr), the drag model fits better to the data. It can be clearly seen that the plume expands adiabatically and reaches farther distances at lower pressures; but at higher pressures it is confined due to the effect of plume-background interaction and mutual interaction between various plasma species. A slight deviation from the drag model is observed in the earlier stages of expansion at 50 Torr, which is probably due to the presence of shock waves at these time scales. To investigate this deviation further, ICCD measurements were repeated at 10 Torr (which is intermediate between 5 Torr and 50 Torr) for two different gate widths: either at a fixed value of 10 ns or at a GW equal to 10% of the GD, such that information loss (if any) occurring in the former measurement is corrected by the latter. As seen from Figure 7, the choice of GW as 10% of GD indeed enhances the measured intensity at larger GDs. Plume intensity is high near the target surface due to plasma confinement at the pressure used (10 Torr). The plume eventually develops a spherical profile even though a fast expansion is seen in the initial stages (≤200 ns).

The R-t plot for an intermediate ambient pressure of 10 Torr is given in Figure 8. As discussed earlier, for sufficiently higher pressures the plasma plume expands soon after irradiation producing shock waves in the surrounding medium. At earlier times of plasma expansion the formation of shock waves alters the plume-front velocity, whereas at later times interaction with the ambient gas curtails plume propagation. Hence, the shock wave model fits in the early stages of expansion and the drag model fits in the later stages, as shown in Figure 8.

Aspect ratio of the plasma plume (ratio of plume length to plume width) is an important parameter which defines its structure and evolution. Aspect ratio is found to be ≥1 in the initial stages of expansion up to about 1 μs (Figure 9), indicating that the plume length is larger than its width. In the later stages of expansion (≥1 μs) aspect ratio is <1, indicating an increasing radial dimension.

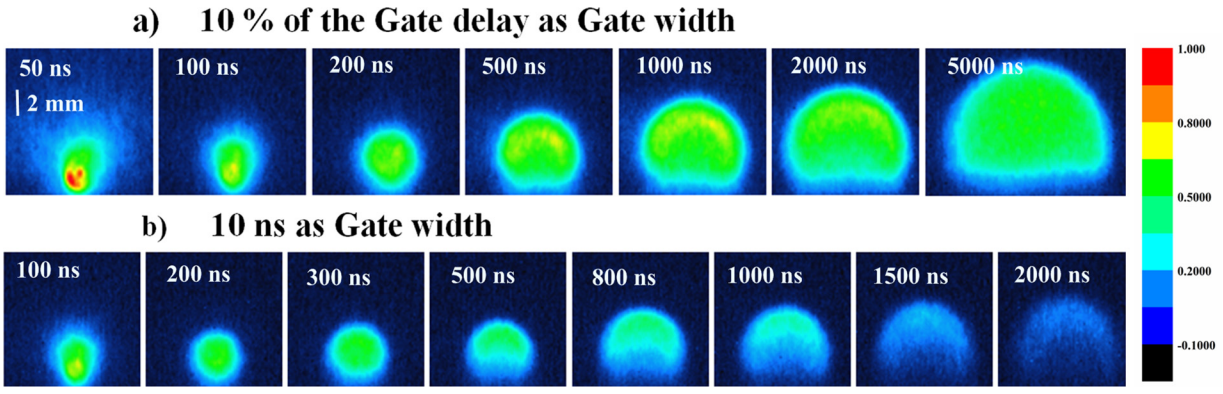

FIG. 7. ICCD images of the plasma plume expanding into 10 Torr nitrogen ambient, measured using (a) 10% of the gate delay as gate width, and (b) 10 ns as gate width.

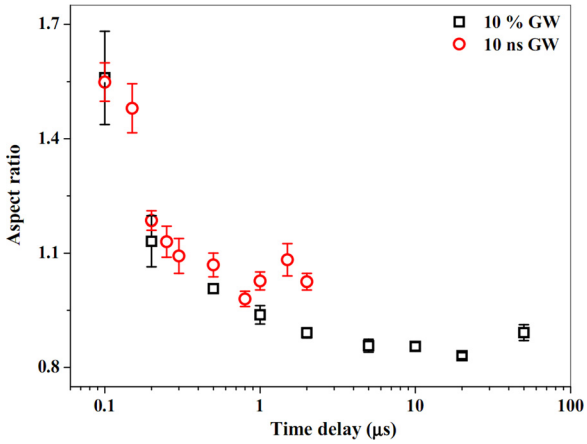

FIG. 9. Aspect ratio of the plume (plume length/plume width) measured at 10 Torr pressure for different ICCD gate widths. Circles are for a gate width of 10 ns, while squares are for a gate width equal to 10% of the gate delay. Aspect ratio decreases over time and goes below 1 around a delay of 1 μs.

IV. CONCLUSION

In conclusion, by using ultrafast laser pulses of 100 fs width obtained from a regeneratively amplified Ti: Sapphire laser, a plasma has been generated on a zinc target, and its optical emission is investigated. Optical time of flight measurements (OTOFs) reveal the dynamics of neutrals and ions in the plasma plume. Measurements show an acceleration of ions in the expanding plasma near the target surface. This acceleration is due to space-charge effects which enhance the internal electric field due to Coulomb forces. Since some of the accelerating ions recombine with slow electrons in the plume to generate neutrals, an acceleration of neutrals also is observed. ICCD measurements carried out at different ambient pressures reveal an expansion dynamics which fits well to theoretical models such as the adiabatic expansion model, shock wave model, and drag model. A transition from the shock wave model at earlier stages of expansion to the drag model at later stages of expansion is observed for intermediate and high ambient pressures. This indicates the role of plasma species interaction and plume-background interaction in limiting plume expansion. These measurements performed at different axial points in the plasma plume for different nitrogen pressures ranging from 0.05 Torr to 100 Torr essentially explore plume velocity variations with space and pressure, and the results are expected to be useful for optimizing plasma parameters for applications like pulsed laser deposition and nanoparticle generation.

ACKNOWLEDGMENTS

Authors are grateful to Professor Ajai Kumar and Mr. Jinto Thomas of the Institute for Plasma Research, Gandhinagar, for access to the ICCD unit.

[1]D. H. Lowndes, D. B. Geohegan, A. A. Puretzky, D. P. Norton, and C. M. Rouleau, Science **273**, 898 (1996).
[2]S. Amoruso, G. Ausanio, R. Bruzzese, M. Vitiello, and X. Wang, Phys. Rev. B **71**, 033406 (2005).
[3]R. A. Ganeev, J. Phys. B: At. Mol. Opt. Phys. **40**, R213 (2007).
[4]D. D. Burgees, B. C. Fawcett, and N. J. Peacock, Proc. Phys. Soc. London **92**, 805 (1967).
[5]D. W. Hahn and N. Omenetto, Appl. Spectrosc. **64**(12), 335A (2010).
[6]C. Phipps, *Laser Ablation and Its Applications* (Springer Science + Business media LLC, 2007).
[7]B. Verhoff, S. S. Harilal, J. R. Freeman, P. K. Diwakar, and A. Hassanein, J. Appl. Phys. **112**, 093303 (2012).
[8]S. Amoruso, G. Ausanio, A. C. Barone, R. Bruzzese, L. Gragnaniello, M. Vitiello, and X. Wang, J. Phys. B: At. Mol. Opt. Phys. **38**, L329 (2005).
[9]S. J. Henley, J. D. Carey, G. M. Fuge, M. N. R. Ashfold, and D. Anglos, Phys. Rev. B **72**, 205413 (2005).
[10]S. I. Anisimov, B. Kapeliovich, and T. Perel'man, JETP **39**, 375 (1994).
[11]S. Amoruso, R. Bruzzese, N. Spinelli, R. Velotta, M. Vitiello, X. Wang, G. Ausanio, V. Iannotti, and L. Lanotte, Appl. Phys. Lett. **84**(22), 4502 (2004).
[12]S. Amoruso, R. Bruzzese, C. Pagano, and X. Wang, Appl. Phys. A **89**, 1017 (2007).
[13]A. Kushwaha and R. K. Thareja, Appl. Opt. **47**(31), G65 (2008).
[14]A. Kumar, R. K. Singh, K. P. Subramanian, B. G. Patel, S. Sunil, and I. A. Prajapati, J. Phys. D: Appl. Phys. **39**, 4860 (2006).
[15]S. George, A. Kumar, R. K. Singh, and V. P. N. Nampoori, Appl. Phys. Lett. **94**, 141501 (2009).
[16]See http://physics.nist.gov/PhysRefData/ASD/lines_form.html for NIST atomic spectra data base.
[17]E. G. Gamaly, A. V. Rode, B. Luther-Davies, and V. T. Tikhonchuk, Phys. Plasmas **9**(3), 949 (2002).
[18]H. Varel, M. Wahmer, A. Rosenfeld, D. Ashkenasi, and E. E. B. Campbell, Appl. Surf. Sci. **127–129**, 128 (1998).
[19]S. S. Harilal, B. O'Shay, M. S. Tillack, and M. V. Mathew, J. Appl. Phys. **98**, 013306 (2005).
[20]T. Gotz and M. Stuke, Appl. Phys. A: Mater. Sci. Process. **64**, 539 (1997), please see http://edoc.mpg.de/261268.
[21]I. Zergioti and M. Stuke, Appl. Phys. A: Mater. Sci. Process. **67**, 391 (1998).
[22]N. Smijesh and R. Philip, J. Appl. Phys. **114**, 093301 (2013).
[23]N. Farid, S. S. Harilal, H. Ding, and A. Hassanein, Appl. Phys. Lett. **103**, 191112 (2013).
[24]N. Smijesh, K. Chandrasekharan, J. C. Joshi, and R. Philip, J. Appl. Phys. **116**, 013301 (2014).
[25]N. Farid, S. S. Harilal, H. Ding, and A. Hassanein, J. Appl. Phys. **115**, 033107 (2014).
[26]S. S. Harilal, C. V. Bindhu, M. S. Tilack, F. Najamabadi, and A. C. Gaeris, J. Appl. Phys. **93**(5), 2380 (2003).
[27]P. T. Rumsby and J. W. M. Paul, Plasma Phys. **16**, 247 (1974).
[28]A. Kumar, R. K. Singh, V. Prahlad, and H. C. Joshi, J. Appl. Phys. **104**, 093302 (2008).
[29]J. H. Whealton and J. C. Whitson, Part. Accel. **10**, 235 (1980), see http://cds.cern.ch/record/1053136/files/p235.pdf.
[30]V. N. Rai, M. Shukla, and H. C. Pant, Laser Part. Beams **18**, 315 (2000).
[31]A. Bazzani, M. Giovannozzi, P. Londrillo, S. Sinigardi, and G. Turchetti, C. R. Méc. **342**, 647 (2014).
[32]H. R. Griem, *Principles of Plasma Spectroscopy* (Cambridge University Press, 1997).
[33]H. Kunze, *Introduction to Plasma Spectroscopy* (Springer-Verlag, Berlin Heidelberg, 2009).
[34]T. Fujimoto, *Plasma Spectroscopy* (Oxford university Press, 2004).
[35]A. Maksimchuk, S. Gu, K. Flippo, D. Umstadter, and V. Yu. Bychenkov, Phys. Rev. Lett. **84**(18), 4108 (2000).
[36]J. F. Keilkopf, Phys. Rev. E **52**, 2013 (1995).
[37]Y. B. Zel'dovich and Y. P. Razier, *Physics of Shock Waves and High Temperature Hydrodynamic Phenomena* (Dover Publications, Inc., Mineola, New York, 2002).
[38]A. E. Hussein, P. K. Divakar, S. S. Harilal, and A. Hassanein, J. Appl. Phys. **113**, 143305 (2013).
[39]W. K. A. Kumuduni, Y. Nakayama, Y. Nakata, T. Okada, and M. Meada, J. Appl. Phys. **74**, 7510 (1993).
[40]J. C. S. Kools, J. Appl. Phys. **74**, 6401 (1993).